

PICOSECOND TRANSIENT GRATING MEASUREMENTS OF SINGLET EXCITON TRANSPORT IN ANTHRACENE SINGLE CRYSTALS

Todd S. ROSE, Roberto RIGHINI[†] and M.D. FAYER

Department of Chemistry, Stanford University, Stanford, California 94305, USA

Received 3 February 1984

Picosecond transient grating experiments are used to measure the rate of exciton transport in anthracene single crystals. The method permits a direct measurement of the transport by introducing an accurate distance scale into the sample. Results from transient grating experiments at 10 K are presented, and the diffusion constant along the \hat{a} crystal axis for the anthracene singlet exciton is reported. Preliminary studies of the temperature dependence of the exciton diffusion constant are also discussed.

1. Introduction

The transport of excitons (electronic excitations) in pure molecular crystals has been under intensive investigation for 50 years [1,2]. In this paper we report the first direct measurement of the rate of exciton transport in a pure molecular crystal. We have investigated singlet exciton transport in anthracene crystals at low temperatures (1.8–20 K) using a picosecond transient grating method [3] which provides a direct observable for the rate of exciton transport along a selected crystallographic direction [4,5].

The application of the picosecond transient grating technique to the investigation of exciton migration works in the following manner [4,5]. A picosecond time scale pulse of light is split in two. The paths of the resulting pulses are arranged to have a known angle between them and to intersect simultaneously in the sample (see fig. 1a). Interference between the two coherently related pulses creates an optical fringe pattern in the sample such that the intensity of light varies sinusoidally in the beam overlap region. The interference fringe spacing is determined by the angle between the beams and by the wavelength of the light.

When the frequency of the exciting light coincides

with an absorption band of the sample molecular crystal, excitations are produced. These excitations will have the same spatial distribution as the sinusoidal optical interference pattern, i.e. there will be a continuous oscillatory variation in the concentration of excited states. After a suitable time delay, a probe pulse (which may differ in wavelength from the exciting pulses) is directed into the sample along a third path. The probe pulse will experience an inhomogeneous optical medium resulting from alternating regions of high and low concentrations of excited states which have different complex indices of refraction [3]. Thus, the probe pulse encounters a *diffraction grating* which causes it to diffract into one or more orders (see fig. 1a). The diffracted pulse leaves the sample along a unique direction. First, consider the case in which exciton migration does not occur. As the excitations which form the induced grating, decay to the ground state, the difference between the indices of refraction of the grating peaks and nulls is reduced. Since the intensity of the diffracted probe pulse depends on the square of the peak–null difference in exciton concentration [3], the diffracted beam decreases in intensity as the time between excitation and probe becomes longer.

Now consider the effect of mobile excitations on the diffracted signal. Migration will move excitons from areas of high exciton concentration, grating

[†] Permanent address: Department of Chemistry, University of Florence, Florence 50121, Italy.

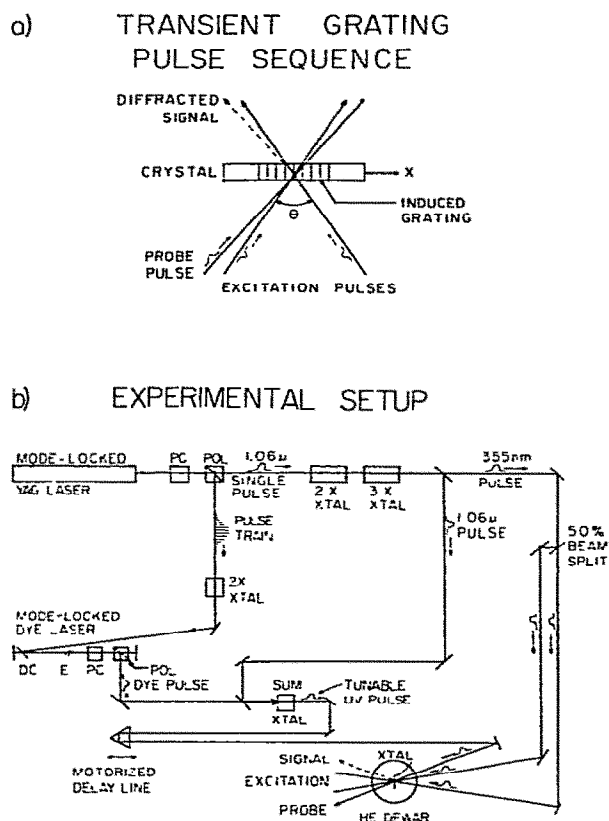


Fig. 1. (a) Schematic illustration of the transient grating experiment. Two coherently related excitation pulses cross in the sample and produce an optical interference pattern. Optical absorption by the sample results in a spatially sinusoidally varying concentration of excited states. This acts as a diffraction grating for the variably delayed probe pulse. Exciton transport, which destroys the grating, is monitored by the time-dependent intensity of the diffracted light. (b) The transient grating experimental arrangement as described in the text. PC \equiv Pockels cell; POL \equiv polarizer; DC \equiv dye cell; E \equiv etalon. A single Nd : YAG $1.06 \mu\text{m}$ picosecond pulse is tripled to 355 nm , beam split, and the resulting pulses are crossed in the sample to produce the transient grating. The left over $1.06 \mu\text{m}$ pulse train is doubled, and the 532 nm pulse train synchronously pumps a dye laser. A cavity-dumped dye laser single pulse is summed with the $1.06 \mu\text{m}$ single pulse to produce a tunable UV probe pulse. Time delay of the probe is achieved with a motorized delay line.

peaks, to areas of low concentration, grating nulls. Thus, the exciton motion will fill in the grating nulls and deplete the peaks. Destruction of the grating pat-

tern by spatial redistribution of the excitations will lead to a decrease in the intensity of the diffracted probe pulse as the probe delay time is increased. Thus the time dependence of the grating signal is directly determined by the rate of exciton transport and by the exciton lifetime.

The transient grating method has several important features. First, the experiment yields the diffusion constant as a direct observable [4,5]. Second, aligning the grating wave vector along a particular crystal direction permits the transport in that direction to be measured. Therefore, anisotropy in transport arising from anisotropy in intermolecular interactions can be investigated. Finally, as discussed below, coherent and diffusive transport generate different characteristic time dependences of the grating signal [4,6]. Diffusive transport yields exponential decays while coherent transport should yield highly non-exponential decays.

In the past, investigations of exciton transport in molecular crystals have involved indirect observables such as exciton trapping or exciton-exciton annihilation. These experiments involve several processes. This leads to problems in extracting transport information from the observables and to wide variations in reports of transport rates obtained from the various indirect techniques [7]. Whatever arguments may be raised in favor of a particular method in a particular system, it is safe to say that there has been no technique capable of directly measuring the rate of exciton transport, as a function of direction, in a wide variety of systems.

In this paper we present experiments which demonstrate that the transient grating method is a tool capable of providing in depth information on exciton transport. Exciton transport along the anthracene \hat{a} crystallographic direction was measured at 20 K, 10 K, and 1.8 K. On the distance scale of the experiments, transport was observed to be diffusive, and the diffusion constants are reported. The rate of transport was found to increase substantially as the temperature was decreased. It is suggested that quasi-coherent transport could account for the observed temperature dependence.

2. Mathematical formulation

The optical interference pattern produces excited

states in the medium such that the initial spatial distribution of excitons along the grating axis (x direction) is given by [3–5]

$$N(x, 0) = \frac{1}{2}(1 + \cos \Delta x), \quad (1)$$

where

$$\Delta = 2\pi/d \quad (2)$$

and d , the grating fringe spacing, is given by

$$d = \lambda/2 \sin(\frac{1}{2}\theta). \quad (3)$$

In eq. (3), λ is the wavelength of the excitation pulses (in air) and θ is the angle between them (in air) (see fig. 1a). A variable time delay probe pulse is diffracted off the induced grating [3]. The diffracted probe is monitored as a function of time delay between the probe and the excitation pulses.

The change in signal, as a function of time (i.e. the decay of the grating), results from two factors: motion of the excitons along the grating axis and lifetime decay. Since the data presented below decay exponentially, we briefly recount the formalism for grating decay arising from diffusive exciton transport [4–6]. The appropriate diffusion equation is

$$\partial N(x, t)/\partial t = D\partial^2 N(x, t)/\partial x^2 - N(x, t)/\tau. \quad (4)$$

In eq. (4), τ is the excited-state lifetime and D is the diffusion constant. $N(x, t)$ describes the distribution of excitons along the grating axis at time t . The solution of the above equation for the initial condition given by eq. (1) is

$$N(x, t) = \frac{1}{2}e^{-t/\tau}(1 + e^{-\Delta^2 D t} \cos \Delta x). \quad (5)$$

The time-dependent grating signal is proportional to the square of the difference, γ , in the exciton concentrations at the grating peaks and nulls [3–5][†]:

$$\gamma(t) = N(0, t) - N(\frac{1}{2}d, t) = \exp[-(\Delta^2 D + 1/\tau)t]. \quad (6)$$

Consequently, the time-dependent signal is

$$S(t) = A[\gamma(t)]^2 = Ae^{-Kt}, \quad (7)$$

where A , a time-independent constant, describes the

strength of the signal and depends on beam geometries, laser intensities, and other experimental factors [3]. For small θ , the decay constant, K , is given by

$$K = 2\Delta^2 D + 2/\tau = (8\pi^2/\lambda^2)\theta^2 D + 2/\tau. \quad (8)$$

It is seen that for diffusive transport, the signal decays exponentially at a rate which depends directly on the diffusion constant in the grating wave vector direction. In principle, if the lifetime is known, the diffusion constant can be obtained from one grating decay measurement at a particular value of θ . In practice, however, it is generally better to evaluate the decay as a function of θ . If transport is responsible for the grating decay, then a plot of K versus θ^2 should yield a straight line. The diffusion constant is obtained from the slope of the line and the lifetime from the y -intercept. This is the procedure employed below.

3. Experimental procedures

The details of the experimental system are schematically illustrated in fig. 1b. The laser is a cw pumped, acousto-optic Q -switched and mode-locked Nd : YAG system which produces 1.06 μm pulse trains at 400 Hz. A single pulse of 130 ps duration and $\approx 40 \mu\text{J}$ in energy is selected by a Pockels cell. The selected single IR pulse is then frequency tripled to produce a 355 nm, 80 ps, 5 μJ TEM₀₀ pulse. The remaining 1.06 μm single pulse is separated from the 355 nm pulse and is summed with a dye laser single pulse. This produces tunable UV pulses, 50 ps in duration. In the experiments, wavelengths in the range 395–400 nm are used. The bandwidth of these pulses is $\approx 2 \text{ \AA}$. The dye laser pulses are derived from a laser, synchronously pumped by the remaining IR pulse train which is frequency doubled before it reaches the dye cell (see fig. 1b).

The 355 nm single pulse is passed through a 50% beamsplitter, and the resulting two pulses are recombined to form the interference pattern. The tunable UV pulse is used as the probe. In some experiments 355 nm is used as the probe and the tunable pulse is beam split and used for grating excitation.

A retroreflector is drawn along a precision optical rail by a motor which provides continuous scanning of the probe delay. A ten-turn potentiometer, also driven by the motor, provides a voltage proportional to the probe delay. This voltage drives the x axis of

[†] Note, subsequent work has shown that the concentration reported in the mixed crystal experiment of ref. [5] is in error. This concentration is the averaged crystal concentration. The experiments, however, were performed on local regions of extremely high, possibly 100%, concentration.

an $x-y$ recorder. The diffracted signal is spatially and spectrally filtered and is detected by a cooled photomultiplier tube and a lock-in amplifier. The output of the lock-in drives the y axis of the recorder. When the delay-line is run, a time-resolved plot of the diffracted signal is obtained.

Prior to crystal growth the anthracene (Aldrich, Gold Label) had been extensively zone-refined and sublimed several times. Care was taken not to expose the compound to white light. Single anthracene sublimation flakes, ranging from 0.5 to 1.7 μm in thickness and averaging 8 mm^2 in area, were grown under 100 Torr of argon (measured at room temperature) at an oil bath temperature of 130°C. The crystals essentially formed two parallel hexagonal faces (ab plane). Their thicknesses were determined by measuring the surface area, dissolving the crystals in a known amount of solvent and measuring the absorption.

The crystals were freely mounted in a holder (similar to that of Philpott et al. [8]) so that the pulses were polarized along the \hat{b} axis and the grating vector pointed along the \hat{a} axis. Fluorescence spectra of the crystals showed sharp lines with virtually no background. This indicated that the crystals were relatively strain free. During the experiment the intensities of the excitation and probe pulses were kept low to avoid crystal damage and saturation effects. The power dependence of the decays in the non-saturation regime was examined over five orders of magnitude. No dramatic effects were observed, and the time dependence of the decays was unaffected. Signal was observed for probe wavelength ranging from 395 to 399 nm. The data displayed below were taken with a probe wavelength of 398.5 nm.

4. Results and discussion

Fig. 2 shows typical decays observed from a single anthracene crystal at 10 K. The upper and lower curves correspond to fringe spacings of 9.6 and 4.1 μm , respectively. The decays, which are exponential, are clearly dependent upon the fringe spacing. A wide fringe spacing is expected to give a slower decay since the excitons must travel farther to affect the grating pattern, while a narrow fringe separation is expected to give a faster decay. In the limit that θ is made extremely small, resulting in a very large fringe spacing,

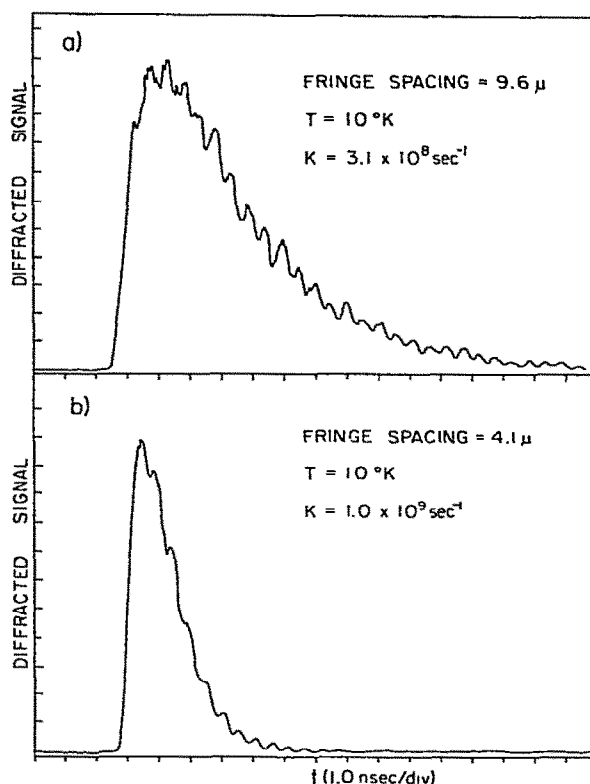


Fig. 2. Typical transient grating decays for an anthracene crystal at 10 K. The upper curve corresponds to a fringe spacing of 9.6 μm and shows a decay constant of $3.1 \times 10^8 \text{ s}^{-1}$. The lower curve was observed for a fringe spacing of 4.1 μm ; the decay constant is $1.0 \times 10^9 \text{ s}^{-1}$. The difference in the decay with fringe spacing arises from exciton transport. As the fringe spacing becomes smaller, it takes less time for the excitons to migrate from grating peaks to grating nulls, resulting in faster decays.

the decay of the signal is dominated by the lifetime. The decays also exhibit prominent oscillations. The modulation results from acoustic effects and will be discussed below.

Figs. 3a and 3b respectively illustrate a typical plot of K versus θ^2 for one crystal and for representative crystals at 10 K. The average diffusion constant, D , obtained from all crystals measured is $1.3 \pm 0.4 \text{ cm}^2/\text{s}$ along the \hat{a} crystal axis; the lifetime is $9 \pm 2 \text{ ns}$. The spread in diffusion constants shown in fig. 3b may represent real differences arising from variations in strain, defect number, or other causes.

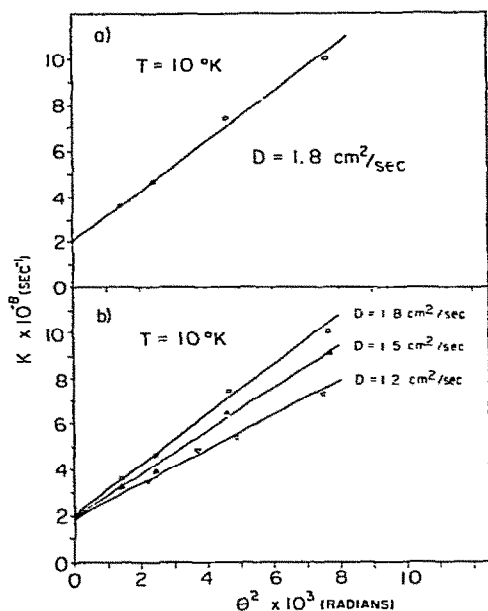


Fig. 3. (a) A typical plot of K versus θ^2 for an anthracene crystal at 10 K, along the \bar{a} axis. The magnitude of the slope equals $8\pi^2 D/\lambda^2$, and thus yields directly the diffusion constant, D . The value of the intercept equals $2/\tau$, where τ is the exciton lifetime. (b) K versus θ^2 for three anthracene crystals at 10 K. Variations among the crystals may be real, arising from differences in strain and other crystal properties. The average diffusion constant obtained from all crystals examined is $D = 1.3 \pm 0.4 \text{ cm}^2/\text{s}$ along the \bar{a} crystal axis.

To test the validity of the measurements, we determined that the decays were independent of power once the power in the pulses had been reduced sufficiently such that the signal was linear in the intensity of each of the three pulses. Excitation pulse energies of a fraction of nanojoule were used with an $\approx 300 \mu\text{m}$ spot size. We found no correlation between crystal thickness and the measured decay constant, indicating that re-absorption is not affecting the measurement of the diffusion constant, although at 10 K, re-absorption is having some effect on the lifetime [9]. We also interchanged the probe and excitation wavelengths, exciting at 395 nm and probing at 355 nm. The diffusion coefficients obtained from two crystals at 10 K were consistent with the data in fig. 3b. This demonstrates that the observed diffusion coefficient (within our current experimental error) is independent of whether the sample is excited above the exciton

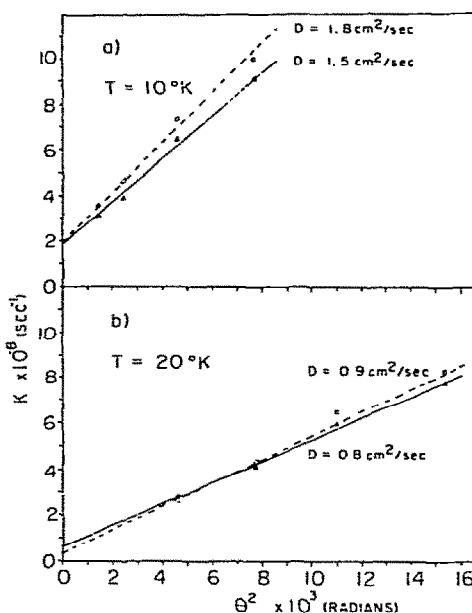


Fig. 4. (a) K versus θ^2 for two crystals at 10 K. (b) K versus θ^2 for the same two crystals at 20 K. The difference in slopes is due to the temperature dependence of the exciton diffusion constant. As the temperature increases, a decrease in the diffusion constant is observed.

band origin and the band is populated by radiationless relaxation, or the band is populated by direct optical excitation. It also shows that the heat deposited by radiationless relaxation does not affect the measurement of the diffusion coefficient.

The diffusion constant exhibits a definite temperature dependence. Figs. 4a and 4b show plots of K versus θ^2 for the same two crystals at 10 and 20 K, respectively. Preliminary experiments have given diffusion constants of approximately $10 \pm 2 \text{ cm}^2/\text{s}$ at 1.8 K and $0.8 \pm 0.2 \text{ cm}^2/\text{s}$ at 20 K. (The lifetime also shows a strong temperature dependence and reaches a value of $\approx 2 \text{ ns}$ at 2 K, consistent with previous reports [9].) In all cases the decays were exponential, demonstrating that on the distance scale of the experiment, $\approx 1 \mu\text{m}$ at the smallest fringe spacing, exciton transport is diffusive.

Although the temperature dependence is preliminary, it is interesting to speculate on its nature. At sufficiently high temperature, transport is describable in terms of the Förster formalism [10], and the diffusion constant can in principle be determined from the overlap between the absorption and emission spectra [10].

This is certainly the case at room temperature. Hopping transport of this type is mildly temperature activated. Then strictly incoherent transport appears to be inconsistent with the observed increase in diffusion constant with decreasing temperature. Although the transient grating decays are exponential, indicating diffusive transport on a $1 \mu\text{m}$ distance scale, coherent transport [2] could nonetheless be responsible for the observed temperature dependence. If at temperature T the exciton has an ensemble average coherence length $\langle l(T) \rangle$, which is long relative to a lattice spacing but short relative to the experimental fringe spacing, ($d = 1 \mu\text{m}$), then the observed decays will be exponential. The exciton ensemble will appear to be executing a random walk with an average step size $\langle l(T) \rangle$. As the temperature decreases, the exciton-phonon scattering rate decreases and $\langle l(T) \rangle$ increases. For a random walk with step size l , the diffusion constant is proportional to l^2 . Therefore, an increase in D is expected as the temperature decreases. This will be offset somewhat by a reduction in the ensemble average exciton group velocity, $\langle V_g(T) \rangle$ [11]. At low temperature, the exciton-phonon scattering rate is reduced, but the group velocity at which an exciton travels between scattering events, on the average, is also reduced. The net result is that the model described here suggests that the temperature dependence of the observable, D , will depend on both the mechanism of exciton-phonon scattering and on the details of the exciton band dispersion.

If the excitons are in fact quasi-coherent with a coherence length $\langle l(T) \rangle$, then for $\langle l(T) \rangle \geq \frac{1}{2}d$ the coherence should manifest itself directly in the functional form of the decays [4,5]. Fringe spacings of $\approx 1000 \text{ \AA}$ are practical, and will be employed in future experiments. However, lineshape data on the anthracene exciton origin [12], if interpreted as an exciton coherence time, suggest that the excitons, even at 1.8 K, are incoherent. This at first appears inconsistent with the observed temperature dependence. However, the absorption lines can be non-locally inhomogeneously broadened from strain or other causes. The relationship of the absorption spectrum to the transport properties is at this time unclear.

The high-frequency oscillations seen in fig. 2 did not change with the grating fringe spacing. This is inconsistent with previously observed laser-induced acoustic diffraction phenomena [3,13]. We propose

that these high-frequency oscillations arise from the repeated reflection of an acoustic disturbance between the front and back surfaces of the crystal. Since the samples have an optical density of ≈ 1 , the front part of the crystal absorbs more of the grating excitation than the back. This non-uniformity could produce a disturbance which reflects back and forth between the crystal faces [14] modulating the grating diffraction efficiency in a time-dependent manner. If this model is correct, the oscillations will occur at a rate which depends on the crystal thickness and the velocity of sound perpendicular to the faces, and not on the grating fringe spacing. This explanation is consistent with the data in fig. 2 which display an oscillation period of 0.5 ns. This is the round trip time for sound traveling at the appropriate velocity, $3.5 \times 10^5 \text{ cm/s}$ [15], over a distance of $0.9 \mu\text{m}$, the thickness of the crystal used for fig. 2, within experimental uncertainty. Furthermore, the period of oscillation varies from crystal to crystal and appears to correspond to the crystal thickness. At this time a quantitative test of this hypothesis is difficult since the crystal dimensions are hard to determine accurately and the experiment is presently limited to a small thickness range.

Acknowledgement

We would like to thank R.J. Dwayne Miller for assistance in the initial stages of these experiments and for making valuable contributions to this effort. This work was supported by the National Science Foundation, Division of Materials Research, Grant number 79-20380. We would also like to acknowledge the Stanford University Center for Materials Research, Grant number 80-20248, for some support which contributed to this research. RR acknowledges a NATO Postdoctoral Fellowship. MDF would like to acknowledge the Simon Guggenheim Memorial Foundation for Fellowship support which contributed to this research.

References

- [1] J. Frenkel, Phys. Rev. 37 (1931) 17, 1276.
- [2] V.M. Agranovich and R.M. Hochstrasser, eds., Spectroscopy and excitation dynamics of condensed molecular systems (North-Holland, Amsterdam, 1983).

- [3] K.A. Nelson, R. Casalegno, R.J.D. Miller and M.D. Fayer, *J. Chem. Phys.* 77 (1982) 1144.
- [4] M.D. Fayer, in: *Spectroscopy and excitation dynamics of condensed molecular systems*, eds. V.M. Agranovich and R.M. Hochstrasser (North-Holland, Amsterdam, 1983) p. 233.
- [5] J.R. Salcedo, A.E. Siegman, D.D. Dlott and M.D. Fayer, *Phys. Rev. Letters* 41 (1978) 131.
- [6] V.M. Kenkre, *Phys. Rev.* B22 (1980) 3072.
- [7] R.C. Powell and Z.G. Soos, *J. Luminescence* 11 (1975) 1.
- [8] J.M. Turllet, Ph. Kottis and M.R. Philpott, *Advan. Chem. Phys.* 54 (1983) 303.
- [9] L.M. Logan, I.H. Munro, D.F. Williams and F.R. Lipsett, *Molecular luminescence* (Benjamin, New York, 1969) p. 773;
- M.D. Galanin, Sh.D. Khan-Magometova and E.N. Mysnikov, *Solid State Commun.* 45 (1983) 739.
- [10] Th. Förster, *Ann. Physik (Leipzig)* 2 (1948) 55.
- [11] D.D. Dlott and M.D. Fayer, *Chem. Phys. Letters* 41 (1976) 305;
- M.D. Fayer and C.B. Harris, *Phys. Rev.* B9 (1974) 748.
- [12] J. Ferguson, *Chem. Phys. Letters* 36 (1975) 316.
- [13] K.A. Nelson, R.J.D. Miller, D.R. Lutz and M.D. Fayer, *J. Appl. Phys.* 53 (1982) 1144;
- R.J.D. Miller, R. Casalegno, K.A. Nelson and M.D. Fayer, *Chem. Phys.* 72 (1982) 371.
- [14] V.L. Broude, *Mol. Cryst. Liquid Cryst.* 57 (1980) 9.
- [15] H.B. Huntington, S.G. Gangoli and J.L. Mills, *J. Chem. Phys.* 50 (1969) 3844.